19th Brazilian Congress of Thermal Sciences and Engineering
November 6th–10th, 2022, Bento Gonçalves - RS - Brazil

ENC-2022-0085
ROLE OF DRAG FORCE IN GRANULAR SIZE SEGREGATION IN SEDIMENT TRANSPORT

Jaime Gonzalez Maya
UNICAMP-University of Campinas, School of Mechanical Engineering, Rua Mendeleyev, 200, Campinas, 13083-860, Brazil
Escuela Politécnica Nacional, Petroleum Department, Quito, 170525, Ecuador
jaime.gonzalez@epn.edu.ec,

Fernando David Cúñez Benalcázar
Department of Earth and Environmental Sciences, University of Rochester,Rochester, NY 14627, USA
fcunezbe@ur.rochester.edu

Erick de Moraes Franklin
UNICAMP-University of Campinas, School of Mechanical Engineering, Rua Mendeleyev, 200, Campinas, 13083-860, Brazil
franklin@fem.unicamp.br

Abstract. *Fluid-driven granular flows are usually found in nature, such as the transport of fine and coarse sediments at the bottom of rivers and the formation of sand dunes in deserts, and have been studied for a while; however, understanding their behavior remains a challenge. In this work, we develop numerical simulations by using an Eulerian-Lagrangian approach, where the fluid flow is solved by Computational Fluid Dynamics (CFD) and the particle interactions are computed by the Discrete Element Method (DEM), being the drag force, which computes the fluid-particles interactions, an important parameter that couples both methods. Thus, this study aims to test and validate different drag force correlations in order to analyze size segregation that coarse grains experience in a dense granular flow. To run the numerical simulations, we used a rectangular channel filled with grains of two different sizes, where, we imposed a Couette laminar fluid flow by moving the top wall of the channel. This induced the motion of particles by bedload, which consists in a thin moving layer in the surface of the granular bed, and creep, which corresponds to a larger layer underneath the bedload layer. To mimic a long infinitely river, we set periodic conditions at the inlet and outlet of the channel in the streamwise direction. Our preliminary results show that coarse grains segregate towards the bed surface from the creep layer, for which we plotted the trajectories of coarse particles over time for different fluid flows conditions. Besides, we analyze the influence of 3 different drag models in our simulations and how they affect the segregation rate. Finally, we also validate our simulations with experiments that have been running lately. Our results will lead us to understand the segregation behavior that may be found in more complex scenarios such as rock river beds.*

Keywords: *sediment transport, size segregation, bedload transport, drag model correlations.*

1. INTRODUCTION

In nature, we can find non-cohesive coarse materials such as sand, gravel, beads, or pebbles that are entrained by the fluid flow,as happens in the bottom of the gravel bed rivers, where these materials are usually transported by processes of small jumps, rolling, and sliding which leads to a thin moving layer in the surface of the granular bed (Bagnold, 1973). This phenomenon is known as bedload transport or sediment transport, which is responsible for diverse river shapes, changes in the coastal morphologies, and the evolution of landscapes. Besides, it involves different spatial-temporal scales: i) large scales such as traversing immense distances for a long time, eroding, transporting, and depositing sediments along the way; ii) small scales as the interaction between particles (sand, gravel, beads, etc.) within the bedload causes the onset of erosion, deposition, and segregation of particles in short or mid time scale (Popović *et al.*, 2021; Lajeunesse *et al.*, 2017; Gallop *et al.*, 2015).Thus, the interactions between the particles within granular beds on small scales influence the transport characteristics on larger scales. However, understanding the behavior from these interactions remains a challenge.

The onset of interaction between the particles in the sediment transport is when an incipient motion is detected due

to shear stresses applied by the fluid ($\vec{\tau}_f$). The incipient motion can be characterized by the Shields number (θ), defined as the ratio between the fluid shear stresses modulus at the top of the granular bed and the apparent weight of a single particle (Shields, 1936). When this number is above a critical value (θ_c), it causes an incipient motion of a few particles. In contrast, up to a value of five times the critical Shields number (θ_c), the particles move in a bedload regime (Bagnold, 1973). Several experimental studies found that the critical Shields number for viscous flows reach a constant value, around 0.12; it was tested for a wide range of particle sizes and fluids, in most cases for mono-dispersed beds (Houssais *et al.*, 2015; Ferdowsi *et al.*, 2017; Ouriemi *et al.*, 2007). However, sediment transport usually involves a wide range of grain sizes (Savage and Lun, 1988), such as at a bi-disperse granular bed where the critical Shields number decreases linearly with the surface fraction of small grains (Houssais and Lajeunesse, 2012). If transporting sediments composed of particles with different diameters, size segregation may appear, therefore understand and predicting segregation is relevant to processes where separation of different species may be either desired or avoided (Fan *et al.*, 2014).

In a bi-disperse sediment, transport it is common to see how coarse particles located inside of the granular bed go toward the surface, this phenomenon being called size segregation, which is characterized by two behaviors, one due to the rapid motion from the bedload layer at the bed surface, that is driven by the fluid shear stresses, whereas the other one is the result of to slow creeping motion far below the surface where the contact forces contribute to granular motion (Aussillous *et al.*, 2013; Houssais *et al.*, 2015, 2016; Ferdowsi *et al.*, 2017). Thus, size segregation can be observed from both rapid and slow granular flow regions, and it can extend from the bottom to the top of the bed (Ferdowsi *et al.*, 2017). Indeed, the bedload layer motion influences the large layer underneath which is called creeping (Houssais *et al.*, 2015). For this reason, as shown above, the segregation in bedload transport depends mainly on the drive of the fluid and its coupling with the particles. Therefore, some experiments and numerical simulations were developed to analyze the behavior of particles both mono-dispersed and bi-dispersed granular beds driven by a fluid.

Experiments and theories show that the laminar bedload is similar to its turbulent counterpart in many respects. Therefore, Charru *et al.* (2004) and Houssais *et al.* (2015) ran experiments using an annular flume to study the evolution of a mono-dispersed granular bed sheared by a viscous Couette flow. Thereby, Charru *et al.* (2004) observed that the bed begins to compact due to the local rearrangement of the particles. In order to understand the erosion and deposition processes at the top of the bed surface, the authors proposed a linear relationship between the compaction of the granular bed and the Shields number. Following the studies of Charru *et al.* (2004), Houssais *et al.* (2015) and Ferdowsi *et al.* (2017) employed refractive-index matching between the fluid and particles (Wright *et al.*, 2017) as the optical technique allowed measurements within the bed. The authors ran experiments from shear rates next to the critical to shear rates high enough to obtain the bedload. Houssais *et al.* (2015) showed that exists a regime called creeping, which appears even for shear rates lower than the threshold for particle motion; this regime usually appears just beneath the bedload layer where grains present a solid-like behavior. The authors also identified a kink point from the velocity profiles, which marks the boundary between the bedload layer and the creeping regions. Similarly, Ferdowsi *et al.* (2017) studied the size segregation experimentally in laminar bedload transport, and concluded that the near-surface layer drives rapidly advective segregation, which is shear rate dependent. The creeping grains beneath the bedload layer give rise to slow but persistent diffusion-dominated segregation. In addition, the authors show that a coarse surface armoring layer develops how large grains are delivered from below; first more rapidly by bedload, and then more slowly by creep. In brief, according to the results mentioned above, the development of a surface armouring due to size segregation (Ferdowsi *et al.*, 2017) will affect the erosion and deposition processes at the top of the bed surface mentioned by Charru *et al.* (2004). Thus, their model could be modified to a transient model for a bi-dispersed granular bed. Consequently, the critical Shields number will also decrease (Houssais and Lajeunesse, 2012).

Together with the experiments, numerical simulations were developed using both discrete and continuum models to reproduce the results discovered in the laboratories and quantify them. Ferdowsi *et al.* (2017) added to his investigation dry granular flow simulations with Discrete Element Models (DEM); moreover Chassagne *et al.* (2020b) developed simulation DEM coupled with Computing Fluid Dynamics (CFD) for turbulent flow in 1D, in a gravity-driven water-free surface flow that induces a downslope shear-driven bi-dispersed granular flow. Both authors modified parameters such as the coefficient of advection-diffusion from Gray and Thornton (2005) continuum modelâĂŹs, which allowed the continuum model to reproduce the discrete simulations quantitatively. In addition, Chassagne *et al.* (2020a) identified four transport regimes of bi-disperse bedload, which depend on the mobility grade which is a consequence of the reduction of the roughness of the underlying small particles that play the role of a conveyor belt for the large particles at the surface. Besides, bi-dispersed granular flow sheared by viscous flow was studied by Vowinckel *et al.* (2021) and Rettinger *et al.* (2022). They computed from their simulations with DEM+CFD the local shear rate of the fluid, particle volume fraction, total shear, and granular pressure, information needed to investigate the rheological behavior from parameters as the viscous number and the inertial number; the first authors set the sediment transport as a pressure-driven Poiseuille flow, whereas the second authors set such as a shear-driven Couette flow. Finally, Zhou *et al.* (2020) analyzed the size segregation downslope of dense granular flow immersed in different fluids using CFD+DEM numerical simulation. The authors defined three fluid regimes and showed that each one exhibits distinct flow dynamics in which different segregation rates were observed, moreover the presence of a viscous fluid effectively diminishes the degree of separation and slows

down segregation. In this study, the boundary conditions and the segregation behaviors are relevant to submarine flows and subareal saturated debris flows, where buoyancy and fluid drag are likewise relevant. As shown above, numerical simulation enables us to analyze the fluid-driven size segregation of a granular bed and study its behavior in both grain scales and overall. Thus, if drag force models are to be included in the numerical setup, then it is crucial to select an accurate drag force correlation that neither underestimates nor overestimate the segregation rate aiming to achieve a good agreement with experimental results obtained in different conditions.

In this work, we test and validate the drag force correlations developed by Gidaspow *et al.* (1991), Koch and Hill (2001), and Di Felice (1994), in order to analyze the size segregation that coarse grains experience in a dense granular flow driven by a viscous fluid by performing numerical simulations through the open source code CFDEM (https://www.cfdem.com/), which couples the open-source codes OpenFOAM (CFD) and LIGGGHTS (DEM). To run the numerical simulations, we designed a rectangular channel filled with grains of two different sizes immersed in a viscous fluid; we imposed a mean velocity at the top of the channel and set periodic conditions at the inlet and outlet of the channel in the streamwise direction, thus mimicking a long infinite river. Finally, we also validated our simulations with experiments that have been running lately.

2. FORMULATION OF THE NUMERICAL MODEL

In this work, we carried out numerical simulations by using an Eulerian-Lagrange approach, where the fluid flow is described by the Navier-Stokes equations for multiphase flows and solved by using the open source code OpenFOAM ($https://www.openfoam.org$); and the discrete phase is computed by using Newton's second law, where each particle interaction is computed based on Discrete Element Method-DEM by using the open source code LIGGGHTS, (Kloss *et al.*, 2012), ($https:/www.liggghts.com$). Finally, OpenFOAM and LIGGGHTS are coupled with the open source code CFDEM (Zhou *et al.*, 2010), ($https://www.cfdem.com/$).

2.1 Governing equations

The two types of particle motion, translational and rotational, are computed based on Newton's second law obtained from the linear and angular momentum equations Eq. (1) and Eq. (2), respectively:

$$m_p \frac{d\vec{u}_p}{dt} = \vec{F}_{fp} + \vec{F}_{pres} + \vec{F}_{vm} + m_p\vec{g} + \sum_{i\neq j}^{N_c}(\vec{F}_{c,ij}) + \sum_{i}^{N_w}(\vec{F}_{c,iw}) \tag{1}$$

$$I_p \frac{d\vec{\omega}_p}{dt} = \sum_{i\neq j}^{N_c}(\vec{T}_{p,ij}) + \sum_{i}^{N_w}(\vec{T}_{p,iw}) \tag{2}$$

where m_p and $\vec{u}_p$ are the mass and the velocity of the particle, respectively. The terms on the right-hand side of Eq. (1) represent the forces generated by the liquid; drag force $\vec{F}_{fp} = -\vec{F}_{pf}$, forces due to pressure and stresses gradients $\vec{F}_{pres} = -V_p\nabla P + V_p\nabla\cdot\vec{\vec{\tau}}_f = V_p\rho_f(\frac{D\vec{u}_f}{D_t} - \vec{g})$ where $(\frac{D\vec{u}_f}{D_t})$ is the material derivative, virtual mass force $\vec{F}_{vm}$, acceleration of gravity $\vec{g}$, contact forces between particles $\vec{F}_{c,ij}$ and contact forces between particles and the tube wall $\vec{F}_{c,iw}$. In Eq. (2), I_p and $\vec{\omega}_p$ are the moment of inertia and angular velocity of a particle, respectively, and the terms on the left-hand side, $\vec{T}_{p,ij}$ represents the torque generated by the tangential component of the contact force between particles *i* and *j*, and $\vec{T}_{p,iw}$ the torque generated by the tangential component of the contact force between particle *i* and the wall. The inter-particle forces and torques are summed over the N_c - 1 particles in contact with particle *i*, where N_c is the total number of particles in contact. The particle-wall forces and torques are summed over the N_w particles in contact with the wall. The contact forces between particles and between particles and the wall are computed based on the soft-particle method (Cúñez and Franklin, 2019).

Locally-averaged incompressible Navier-Stokes equations compute velocity and pressure fields. The mass and momentum equations are given by Eqs. (3) (4), respectively:

$$\frac{\partial\rho_f\alpha_f}{\partial t} + \nabla\cdot(\rho_f\alpha_f\vec{u}_f) = 0 \tag{3}$$

$$\frac{\partial\rho_f\alpha_f\vec{u}_f}{\partial t} + \nabla\cdot(\rho_f\alpha_f\vec{u}_f\vec{u}_f) = -\alpha_f\nabla P + \alpha_f\nabla\cdot\vec{\vec{\tau}}_f + \alpha_f\rho_f\vec{g} + \vec{F}_{pf} \tag{4}$$

where P is the pressure, $\vec{\vec{\tau}}_f$ is the stresses tensor, and $\vec{u}_f$ and α_f represent the mean velocity and volume fraction of the fluid phase, respectively. Coupling between liquid phase and particles is achieved through the momentum exchange coefficients $\vec{F}_{pf}$, (Li *et al.*, 2017), and it can be computed by Eq. (5)

$$\vec{F}_{pf} = \frac{1}{V_{cell}}\sum_{\forall_p\in_{cell}}\frac{V_p\beta}{1-\in_f}(\vec{u}_p - \vec{u}_{fp}) \tag{5}$$

where V_{cell} and V_p are the volumes of the considered cell and particle, respectively, β is the coefficient of momentum transfer between phases due to the drag force, it can be calculated from some correlations as Eq.6, Eq.8 or Eq.10, which were tested in this work, finally $\vec{u}_{fp}$ is the liquid velocity at the particle position. The latter is usually obtained by interpolation and determined for each particle.

2.2 Drag forces correlations

The main momentum exchange coefficient between a fluid phase and solid particles is the drag force, which in dense systems has a complex dependency on the porosity, which coincide with the V_{cell} liquid volume fraction α_f, and on the particle Reynolds number; $Re_{p(s,l)} = (\alpha_f d_{p(s,l)}|\vec{u}_p - \vec{u}_f|)/\nu$, the subscripts *s* and *l* denoting large and small particle, respectively. Several works were developed to find correlations of coefficient of momentum transfer β. We tested the following formulations.

Gidaspow *et al.* (1991), developed a correlation that allows to work well in both dense and in dilute regions

$$\beta = \begin{cases} \frac{3}{4} C_D \frac{\rho_f (1-\alpha_f)(|\vec{u}_{p(s,l)} - \vec{u}_f|)}{d_{p(s,l)}} \alpha_f^{-1.65} & for \quad \alpha_f \geq 0.8 \\ 150 \frac{(1-\alpha_f)^2 \mu}{\alpha_f (d_{p(s,l)})^2} + 1.75 \frac{\rho_f (1-\alpha_f)(|\vec{u}_{p(s,l)} - \vec{u}_f|)}{d_{p(s,l)}} & for \quad \alpha_f < 0.8 \end{cases} \tag{6}$$

where;

$$C_D = \frac{24}{Re_{p(s,l)}} [1 + 0.15 (Re_{p(s.l)})^{0.687}]. \tag{7}$$

Koch and Hill (2001), proposed a correlation on the basis of Lattice-Boltzmann simulations of fluid flows through arrays of spheres

$$\beta = 18 \alpha_f (F_0 + 0.5 F_1 \alpha_1 Re_{p(s,l)}) \tag{8}$$

where;

$$F_0 = \begin{cases} \frac{1+3((1-\alpha_f)/2)^{1/2} + 135/64 (1-\alpha_f) ln(1-\alpha_f) + 16.14 (1-\alpha_f)}{1+0.681(1-\alpha_f) - 8.48 (1-\alpha_f)^2 + 8.16 (1-\alpha_f)^3} & for \quad (1-\alpha_f) \leq 0.4 \\ \frac{10(1-\alpha_f)}{(1-\alpha_f)^3} & for \quad (1-\alpha_f) > 0.4 \end{cases} \tag{9}$$

$$F_1 = 0.0673 + 0.212 (1-\alpha_f) + 0.0232 (1-\alpha_f)^{-5}. \tag{10}$$

Di Felice (1994), considered data from several systems and showed that the coefficient of a α_f should not be constant but should instead be a function of the particle Reynolds number.

$$\beta = 0.75 C_D Re_{p(s,l)} \alpha_f^{2-\lambda} \tag{11}$$

where

$$C_D = \left(0.63 + \frac{4.8}{\sqrt{\alpha_f Re_{p(s,l)}}} \right)^2 \tag{12}$$

$$\lambda_{DiFelice} = 3.7 - 0.65 exp \left(- \frac{\left(1.5 - \log (\alpha_f Re_{p(s,l)})\right)^2}{2} \right). \tag{13}$$

2.3 Numerical setup

The 3D channel has dimension of length, width, and height of $50 d_s \times 20 d_s \times 15 d_s$, whereas large particles of diameter d_l = 3 mm and small particles of diameter d_s = 2 mm (size ratio d_l/d_s = 1.5) are deposited randomly by gravity inside a channel, in order to form a 24 mm fixed bed with 10236 particles (volume ratio V_s/V_l = 1.75), see Fig. 1a. The particle and fluid densities are fixed respectively as ρ_p = 2500 kgm^{-3} and ρ_f = 1400 kgm^{-3}, and the viscosity is $\nu = 6 \times 10^{-4}$ m^{2}s^{-1}, these properties correspond to glass spheres and a sodium iodide (NaI) solution at 35% (w/w) in glycerin, respectively. We set periodic boundary conditions in the stream-wise (x), and no-slip condition both on the bottom and lateral walls of the channel. We imposed a Couette laminar flow setting up a mean velocity of u_{top} = 0.083 ms^{-1} at the top of the channel. The section of liquid above the bed measure h_f = 6 mm, in these condition we calculated: The Reynolds number based on the height of the fluid is $Re = u_f h_f / \nu$ = 0.97 and the Shields number $\theta = \tau_f / (g d_s (\rho_p - \rho_f))$ = 0.45 for small particles. All simulations were executed for 200 seconds in a hexahedral coarse domain of size $L_x \times L_y \times L_z = 40 \times 17 \times 20$ cells.

Table 1. The parameters for discrete element method (DEM)

Parameters	Value
Young's modulus of glass beads E$^{(1)}$	0.46×10^9 GPa
Poisson/s ratio of glass beads $\nu^{(1)}$	0.245
Friction coefficient between glass bead particles Âţ	0.60
Restitution coefficient between glass bead particles COR$^{(2)}$	0.051

$^{(1)}$ (Tang *et al.*, 2019)
$^{(2)}$ (Gollwitzer *et al.*, 2012)

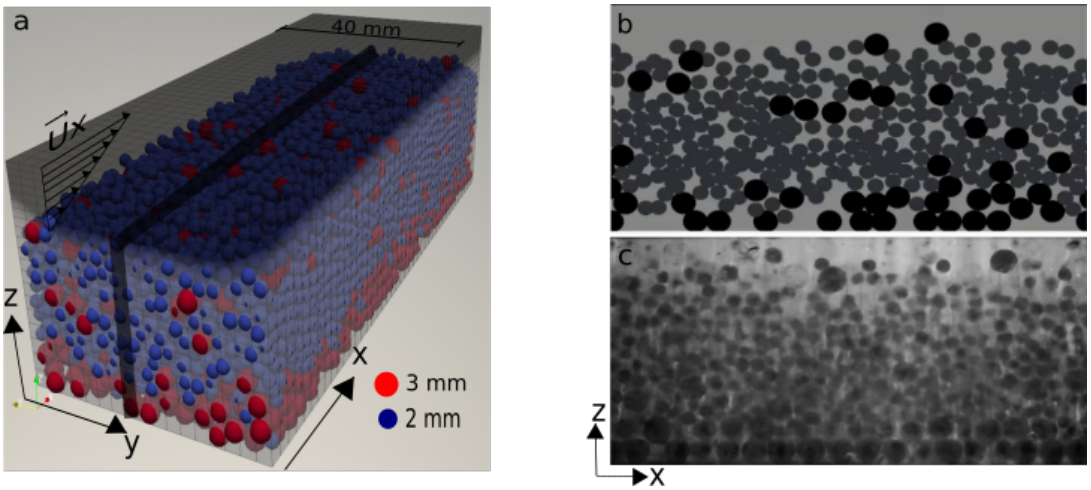

Figure 1. a) 3D view of the of physical setup; b) Vertical profile of the granular bed from simulations; c) A slice of the granular bed from the experiments

3. RESULTS

We compare the numerical results with the data from experiments that we have been running lately in a closed-top annular flume, which through the use of refractive-index matching techniques allows us to obtain images of a vertical profile of grains (Gonzalez *et al.*, 2021), as shown in the Fig.1b. We estimate the particle velocity frame by frame by using the Lagrangian particle tracking from Ouellette *et al.* (2006) that stitch positions at different frames into tracks. For this work, the running time of experiment was 10 min.

We can see in Fig. 1c a slice from the center of the 3D channel. Both the experimental and numerical vertical profile of the granular bed shows a qualitative similarity. However, the role that the drag models play on a granular bed affects, directly and indirectly, the bedload layer and the layers beneath it, respectively.

3.1 Role of the drag forces

As shown in the equations, the various force definitions only differ in the dependency on the porosity, which coincides with the V_{cell} liquid volume fraction α_f and the particle Reynolds number $Re_{p(s,l)}$. The solid (and hence fluid) packing fraction can be observed from Fig. 1b and Fig. 2a its ranges within the bedload layer vary from dilute to dense concentration, where the values of solid packing fraction are between 0.1 up to 0.5; while from the layers beneath the bed load layer to bottom is quite constant, comparable to a packed bed, with solid volume fraction values of about 0.6. Particle Reynolds number has more influence mainly on the surface of the bedload layer than on the underlayers where the threshold of the motion is found. However, the velocity gradient decreases linearly from the channel lid to the granular bed surface, its influence affects the erosion and deposition processes of particles on the bed, due to the presence of small jumps, collisions, and sliding of particles, where the particle Reynolds number has significant variations. Thus, both the effect of the packing concentration and particle Reynolds number in the drag force correlations have major consequences on the surface of a bi-dispersed granular bed surface, due to an increase in the packing fraction and variation of particle diameter, being the segregation rate of coarse particle towards the surface of the granular bed the result more visible. Figures 2b and 2c, show the snapshot of channel cross-section view only with coarse particles; before segregating and after segregating, respectively. The empty areas are occupied by fine particles, which segregated downwards through kinetic sieving processes.

We calculate the spatial-time-average velocity magnitude for the three drag forces correlation tested, and plot it with

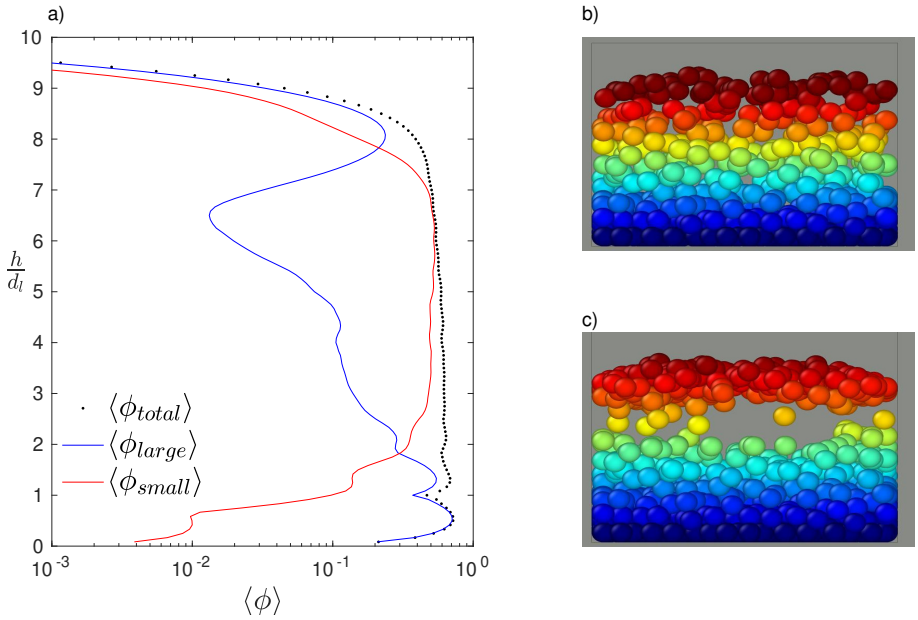

Figure 2. a) Packing fraction; b) Snapshot of channel cross-section view, before segregation; c) after segregation

respect to height channel, these velocity profiles of the granular bed are shown in the Fig. 3a and contrasted with experimental data. We can see that none of the models can give a perfect prediction of the granular bed velocity profiles. Nonetheless, The DiFelce model seems to represent the best results considering the bedload layer region, where both the porosity and the particle Reynolds number have a wide range of values. The Gidaspow and Koch-Hill models behave similarly in this region with velocities higher than the experiments; it means more mobility on the surface of granular bed. Overall, all models overestimate (around one magnitude order) the velocity value in the layer beneath the bedload layer as a consequence of the great mobility within the bedload layer. As result, the segregation of coarse particles towards the surface bed is faster in the simulation than the observed in the experiments. The behavior of the velocity, mainly in the layers beneath the bedload layer, can be improved by implementing a smoothing of exchange fields (e.g., particle volume fraction, drag force), that dampen local fluctuations of the fluid volume fraction α_f calculated in neighboring CFD cells, an isotropic diffusive smoothing is applied (Blais *et al.*, 2016; Pirker *et al.*, 2011). This smoothing method is chosen because it is conservative, easy to implement, and can be easily controlled via the smoothing length. The Fig. 2b shows the velocity profile of the granular bed for different smoothing length values evaluated, where s = 2dp$_s$ is sufficient to improve the results of all simulations.

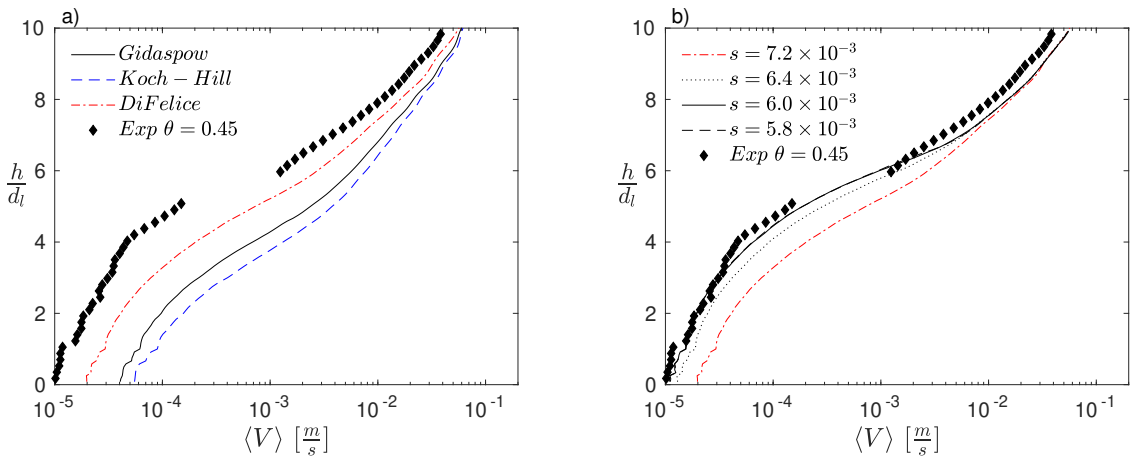

Figure 3. Spatial-time-average of the stream-wise velocity profile, solid and dashed lines are from simulations and dotted lines is from experiment: a) Drag force correlations; b) Smoothing length coefficient by DiFelice drag model

3.2 Size segregation

The particles marked with the red color shown in the Fig. 4b were selected considering the localization within the granular bed from the surface to half of the bed and numerated ascending from one to five, being the number one the particle more close to the surface. Figure 4a shows that only particle number five did not segregate showing an imperceptive displacement throughout the simulation time, while the other particles segregated to the surface of the bed, the number one showed fast segregation, whereas the others manifested moderate segregation. The coarse particles segregated from below towards the surface of the granular bed undergoing several processes at different time scales; they depend on the depth at which the particles are found with respect to the bed surface, see Fig. 4b. Thereby, three regions are observed from Fig. 4a; i) fast, ii) moderate, and iii) slow segregation. The first one has a direct influence of shear stresses by fluid, which leads to instant segregation combined with fragile contact forces between particles, besides the drag force calculated from DiFelice correlation. In this region, small jump, sliding, and rolling processes are present. Moderate segregation is located at the underlayers of the previous one, they correspond to the deeper layers within the bedload layer, it is a collisionless region where the contact forces are moderate, where both the sliding and rolling processes between particles lead to the segregation with a low influence of shear stresses. The last one, slow segregation, is located at the layers beneath the bedload layer (creeping), where the stronger contact forces are found, their intensity and direction lead to the segregation towards the next over layer. Thus, the particles in this region need a long enough time to reach the bed surface. Finally, these processes also match the kinetic sieving the fine particles, which percolates through a moving bed due to a difference in the particle's size, which results in a downward flux of the smaller particles.

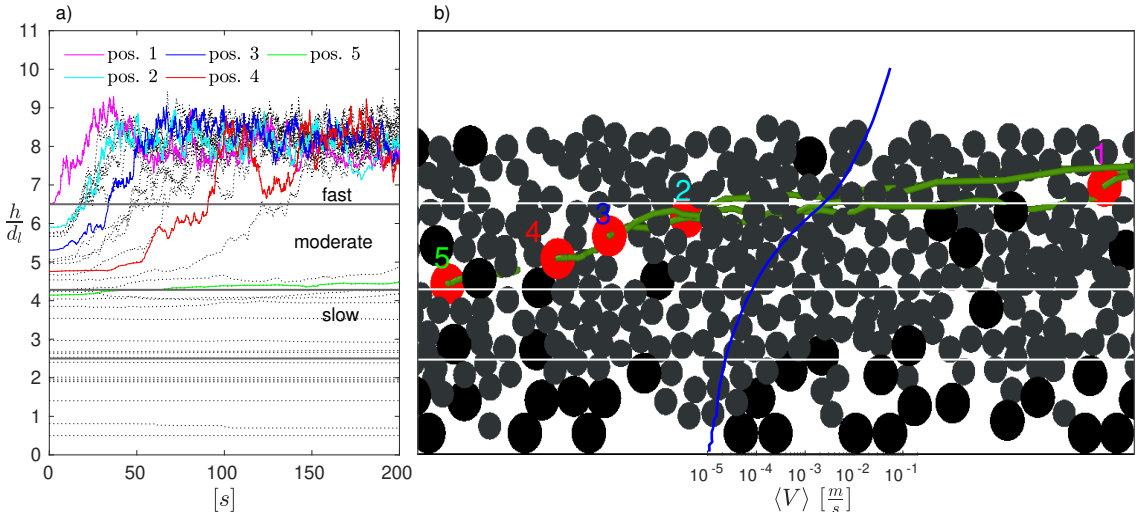

Figure 4. Mobility regions in a granular bed flow and segregation: a) Trajectories of red particles colored in b), showing a vertical profile of the onset granular bed, blue solid line is the velocity profile and green solid lines are the trajectories

4. CONCLUSIONS

We tested three drag force models to investigate their role in granular size segregation in sediment transport. The model of Di Felice (1994) with the addition of the smoothing length coefficients showed a good agreement with experimental data from the spatial-time-average stream-wise velocity profile. We observed that the velocity within the bed is directly related to the creeping region (where velocity is negligible) and bedload layer (where there is noticeable movement). Thus, the segregation of coarse particles was more noticeable within the bedload layer where the drag force is directly involved.

5. ACKNOWLEDGEMENTS

Jaime Gonzalez Maya thanks to the Petroleum Department at Escuela Politécnica Nacional, Quito-Ecuador, Fernando David Cúñez Benalcázar is grateful to FAPESP (Grants no. 2016/18189-0, and 2018/23838-3), and Erick de Moraes Franklin would like to express his gratitude to FAPESP (Grant No. 2018/14981-7).

6. REFERENCES

Aussillous, P., Chauchat, J., Pailha, M., Médale, M. and Guazzelli, E., 2013. "Investigation of the mobile granular layer in bedload transport by laminar shearing flows". *Journal of Fluid Mechanics*, Vol. 736, pp. 594–615.

Bagnold, R.A., 1973. "The nature of saltation and of bedload transport in water". *Proceedings of the Royal Society of London. A. Mathematical and Physical Sciences*, Vol. 332, No. 1591, pp. 473–504.

Blais, B., Lassaigne, M., Goniva, C., Fradette, L. and Bertrand, F., 2016. "Development of an unresolved cfdâĂŞdem model for the flow of viscous suspensions and its application to solidâĂŞliquid mixing". *Journal of Computational Physics*, Vol. 318, pp. 201–221. ISSN 0021-9991. doi:https://doi.org/10.1016/j.jcp.2016.05.008. URL https://www.sciencedirect.com/science/article/pii/S0021999116301358.

Charru, F., Mouilleron, H. and Eiff, O., 2004. "Erosion and deposition of particles on a bed sheared by a viscous flow". *Journal of Fluid Mechanics*, Vol. 519, pp. 55–80. ISSN 00221120. doi:10.1017/S0022112004001028.

Chassagne, R., Frey, P., Maurin, R. and Chauchat, J., 2020a. "Mobility of bidisperse mixtures during bedload transport". *Physical Review Fluids*, Vol. 5, No. 11, p. 114307.

Chassagne, R., Maurin, R., Chauchat, J. and Gray, J.M.N.T., 2020b. "Discrete and continuum modelling of grain size segregation during bedload transport". *J. Fluid Mech*, Vol. 895, No. A30, pp. 1–30. doi:10.1017/jfm.2020.274.

Cúñez, F.D. and Franklin, E., 2019. "Plug regime in water fluidized beds in very narrow tubes". *Powder Technology*, Vol. 345, pp. 234–246. ISSN 1873328X. doi:10.1016/j.powtec.2019.01.009.

Di Felice, R., 1994. "The voidage function for fluid-particle interaction systems". *International journal of multiphase flow*, Vol. 20, No. 1, pp. 153–159.

Fan, Y., Schlick, C.P., Umbanhowar, P.B., Ottino, J.M. and Lueptow, R.M., 2014. "Modelling size segregation of granular materials: the roles of segregation, advection and diffusion". *Journal of fluid mechanics*, Vol. 741, pp. 252–279.

Ferdowsi, B., Ortiz, C.P., Houssais, M. and Jerolmack, D.J., 2017. "River-bed armouring as a granular segregation phenomenon". *Nature Communications*, Vol. 8, pp. 1–10. ISSN 20411723. doi:10.1038/s41467-017-01681-3. URL http://dx.doi.org/10.1038/s41467-017-01681-3.

Gallop, S.L., Collins, M., Pattiaratchi, C.B., Eliot, M.J., Bosserelle, C., Ghisalberti, M., Collins, L.B., Eliot, I., Erftemeijer, P.L., Larcombe, P. *et al.*, 2015. "Challenges in transferring knowledge between scales in coastal sediment dynamics". *Frontiers in Marine Science*, Vol. 2, p. 82.

Gidaspow, D., Bezburuah, R. and Ding, J., 1991. "Hydrodynamics of circulating fluidized beds: kinetic theory approach". Technical report, Illinois Inst. of Tech., Chicago, IL (United States). Dept. of Chemical âĂę.

Gollwitzer, F., Rehberg, I., Kruelle, C.A. and Huang, K., 2012. "Coefficient of restitution for wet particles". *Physical Review E*, Vol. 86, No. 1, p. 011303.

Gonzalez, Jaime, Cúñez, F.D. and Franklin, E., 2021. "Experimental investigation size particles segregation by laminar shearing flows". *COBEM Conference Proceedings*, Vol. 26, No. 1970. doi:10.26678/ABCM.COBEM2021.COB2021-1970.

Gray, J. and Thornton, A., 2005. "A theory for particle size segregation in shallow granular free-surface flows". *Proceedings of the Royal Society A: Mathematical, Physical and Engineering Sciences*, Vol. 461, No. 2057, pp. 1447–1473.

Houssais, M. and Lajeunesse, E., 2012. "Bedload transport of a bimodal sediment bed". *Journal of Geophysical Research: Earth Surface*, Vol. 117, No. F4.

Houssais, M., Ortiz, C.P., Durian, D.J. and Jerolmack, D.J., 2015. "Onset of sediment transport is a continuous transition driven by fluid shear and granular creep". *Nature communications*, Vol. 6, No. 1, pp. 1–8.

Houssais, M., Ortiz, C.P., Durian, D.J. and Jerolmack, D.J., 2016. "Rheology of sediment transported by a laminar flow". *Physical Review E*, Vol. 94, No. 6, p. 062609.

Kloss, C., Goniva, C., Hager, A., Amberger, S. and Pirker, S., 2012. "Models, algorithms and validation for opensource dem and cfd–dem". *Progress in Computational Fluid Dynamics*, Vol. 12, pp. 140–152. doi:10.1504/PCFD.2012.047457.

Koch, D.L. and Hill, R.J., 2001. "Inertial effects in suspension and porous-media flows". *Annual Review of Fluid Mechanics*, Vol. 33, No. 1, pp. 619–647.

Lajeunesse, E., Devauchelle, O., Lachaussée, F. and Claudin, P., 2017. "Bedload transport in laboratory rivers: the erosion-deposition model". *Gravel-bed Rivers: Gravel Bed Rivers and Disasters, Wiley-Blackwell, Oxford, UK*, pp. 415–438.

Li, L., Li, B. and Liu, Z., 2017. "Modeling of spout-fluidized beds and investigation of drag closures using openfoam". *Powder Technol*, Vol. 305, pp. 364–376. ISSN 1873328X.

Ouellette, N.T., Xu, H. and Bodenschatz, E., 2006. "A quantitative study of three-dimensional lagrangian particle tracking algorithms". *Experiments in Fluids*, Vol. 40, No. 2, pp. 301–313.

Ouriemi, M., Aussillous, P., Medale, M., Peysson, Y. and Guazzelli, É., 2007. "Determination of the critical shields number for particle erosion in laminar flow". *Physics of Fluids*, Vol. 19, No. 6, p. 061706.

Pirker, S., Kahrimanovic, D. and Goniva, C., 2011. "Improving the applicability of discrete phase simulations by smoothening their exchange fields". *Applied Mathematical Modelling*, Vol. 35, No. 5, pp. 2479–2488. ISSN 0307-904X. doi:https://doi.org/10.1016/j.apm.2010.11.066. URL https://www.sciencedirect.com/science/article/pii/S0307904X10004762.

Popović, P., Devauchelle, O., Abramian, A. and Lajeunesse, E., 2021. "Sediment load determines the shape of rivers".

Proceedings of the National Academy of Sciences, Vol. 118, No. 49.

Rettinger, C., Eibl, S., Rüde, U. and Vowinckel, B., 2022. "Rheology of mobile sediment beds in laminar shear flow: effects of creep and polydispersity". *Journal of Fluid Mechanics*, Vol. 932.

Savage, S. and Lun, C., 1988. "Particle size segregation in inclined chute flow of dry cohesionless granular solids". *Journal of fluid mechanics*, Vol. 189, pp. 311–335.

Shields, A., 1936. "Anwendung der aehnlichkeitsmechanik und der turbulenzforschung auf die geschiebebewegung". *PhD Thesis Technical University Berlin*.

Tang, H., Song, R., Dong, Y. and Song, X., 2019. "Measurement of restitution and friction coefficients for granular particles and discrete element simulation for the tests of glass beads". *Materials*, Vol. 12, No. 19, p. 3170.

Vowinckel, B., Biegert, E., Meiburg, E., Aussillous, P. and Guazzelli, É., 2021. "Rheology of mobile sediment beds sheared by viscous, pressure-driven flows". *Journal of Fluid Mechanics*, Vol. 921.

Wright, S.F., Zadrazil, I. and Markides, C.N., 2017. "A review of solid–fluid selection options for optical-based measurements in single-phase liquid, two-phase liquid–liquid and multiphase solid–liquid flows". *Experiments in Fluids*, Vol. 58, No. 9, pp. 1–39.

Zhou, G.G., Cui, K.F., Jing, L., Zhao, T., Song, D. and Huang, Y., 2020. "Particle size segregation in granular mass flows with different ambient fluids". *Journal of Geophysical Research: Solid Earth*, Vol. 125, No. 10, p. e2020JB019536.

Zhou, Z.Y., Kuang, S.B., Chu, K.W. and Yu, A.B., 2010. "Discrete particle simulation of particle–fluid flow: model formulations and their applicability". *Journal of Fluid Mechanics*, Vol. 661, pp. 482–510. doi: 10.1017/S002211201000306X.

7. RESPONSIBILITY NOTICE

The following text, properly adapted to the number of authors, must be included in the last section of the paper: The author(s) is (are) solely responsible for the printed material included in this paper.